Atmospheric Environment 350 (2025) 121119

Contents lists available at ScienceDirect

Atmospheric Environment

journal homepage: www.elsevier.com/locate/atmosenv

Vertical profiles of N_2O_5-related chemical species over Seoul, Korea: Modeling approach and implications for aircraft campaign

Hyun-Young Jo [a], Hyo-Jung Lee [b], Gookyoung Heo [c,**], Cheol-Hee Kim [a,b,*]

[a] Institute of Environmental Studies, Pusan National University, Busan, 46241, Republic of Korea
[b] Department of Atmospheric Sciences, Pusan National University, Busan, 46241, Republic of Korea
[c] Environmental Satellite Center, Now at Air Quality Research Division, National Institute of Environmental Research, Incheon, 22689, Republic of Korea

HIGHLIGHTS

- N_2O_5 chemistry is well associated with nocturnal residual layer
- Nitrate radical simulated active at 700–800m in the residual layer at night
- N_2O_5 max. was 200–300 m lower than nitrate radical due to NO_2 profile
- Campaigns may reference simulated vertical profiles for flying altitudes

ARTICLE INFO

Keywords:
Heterogeneous N_2O_5 chemistry
Vertical structures of N_2O_5
Campaign studies
Nocturnal boundary layer
Nitrate aerosol
WRF-CMAQ model

ABSTRACT

Heterogeneous dinitrogen pentoxide (N_2O_5) is an important reactive intermediate in the atmospheric nighttime oxidization of nitrogen oxides and in the formation of nitrate (NO_3^-) aerosols. However, vertical profiles of N_2O_5-related chemical species over Seoul Metropolitan Area (SMA) are currently lacking. In this study, the Weather Research and Forecasting-Community Multiscale Air Quality (WRF-CMAQ) model was employed and simulated vertical profiles of nighttime N_2O_5-related chemical species to facilitate aircraft-based campaigns over the SMA. The vertical structures of the NO_3 radical ($NO_3\bullet$) and N_2O_5 were assessed during the meteorologically stagnant period (March 16–17, 2016), which was a typical period of nighttime N_2O_5-driven NO_3^- formation in the study region. The results showed that nighttime vertical structures exhibiting higher concentrations of N_2O_5-related chemical species were strongly associated with the nocturnal residual layer (RL), which was decoupled from the ground. Our model showed diminished nighttime $NO_3\bullet$ at the ground but active $NO_3\bullet$ aloft, as it was retained in the RL. We also carried out the same analysis for the stagnant period (May 16–22, 2016) during the KORUS-AQ campaign, and confirmed the similar profiles of high concentration of $NO_3\bullet$ near the altitude of RL. To sum up the cases from this study and KORUS-AQ campaign study, maximum nighttime $NO_3\bullet$ and N_2O_5 concentrations occurred at heights of $78 \pm 11\%$ of RL height and $54 \pm 15\%$ of RL height, respectively. Although further research on nighttime N_2O_5 chemistry is needed to resolve outstanding uncertainties, the vertical structures of nighttime N_2O_5-related chemical species obtained in this study offer useful reference data for future aircraft campaigns.

1. Introduction

Particulate matter (PM) studies conducted over the Korean Peninsula have included aircraft campaigns aimed at measuring upper atmospheric PM pollutants at high altitudes. Many such studies have investigated transboundary transport from upstream areas in northeastern Asia, and their results have shown that PM and its precursors remain aloft for ~1.5–3 km during long-distance transport over vast regions such as the Yellow Sea and Korean Peninsula (Kim et al., 2018; Lee et al., 2022; Oh et al., 2020). Elevated PM levels over the Korean

---

* Corresponding author. Department of Atmospheric Sciences, Pusan National University, 30 San, Jangjeon-Dong, Geumjeong-Gu, Busan, 609-735, Republic of Korea.
** Corresponding author. Environmental Satellite Center, Now at Air Quality Research Division, National Institute of Environmental Research, Incheon, 22689, Republic of Korea.
E-mail addresses: gookyoung.heo@gmail.com (G. Heo), chkim2@pusan.ac.kr (C.-H. Kim).

https://doi.org/10.1016/j.atmosenv.2025.121119
Received 7 September 2024; Received in revised form 15 January 2025; Accepted 19 February 2025

Peninsula and Seoul Metropolitan Area (SMA) have been the focus of several aircraft-based air quality studies performed in combination with surface observations, including the Megacity Air Pollution Studies–Seoul (MAPS–Seoul) in 2015, Korea–United States Air Quality (KORUS–AQ) in 2016, Satellite Integrated Joint Monitoring for Air Quality (SIJAQ) in 2021–2022, and Airborne and Satellite Investigation of Asian Air Quality (ASIA-AQ) in 2024. The resulting aircraft-based measurements together with satellite images and modeling results have been employed to explore many issues related to atmospheric PM over Korean Peninsula (Chang et al., 2022; Crawford et al., 2021; Jo et al., 2023; Kim et al., 2023; Lee et al., 2019; Oh et al., 2024; Park et al., 2018, 2021; Park and Kim, 2021).

Nighttime secondary $PM_{2.5}$ levels have also been investigated due to the possibility of high rates of nighttime $PM_{2.5}$ formation through chemical species related to heterogeneous dinitrogen pentoxide (N_2O_5), in which NO_3^- aerosols are formed mainly via the heterogeneous N_2O_5 hydrolysis pathway (Brown et al., 2006a, 2006b, 2016; Finlayson-Pitts and Pitts, 2000; Kim et al., 2014; Ravishankara, 1997; Yun et al., 2024). During the night, nitrate radical ($NO_3\bullet$) production is generally zero at surface, due to the absence of sunlight, albeit with high surface NO_x emissions. However, although nighttime N_2O_5 can act as a reservoir of NO_x and O_3 in the upper atmosphere, nighttime N_2O_5 chemistry remains poorly understood.

The nature of the atmospheric boundary layer (ABL) differs between day and night. During the day, the ABL is vertically well mixed due to vigorous turbulence under daytime convective conditions (Lee et al., 2023; Stull, 1988; Lu et al., 2019). At night, however, turbulence weakens and an inversion develops from the surface due to strong radiative cooling. At night, the formation of a stable nocturnal boundary layer (NBL) hinders vertical mixing and allows the formation of a residual layer (RL) above it. The RL is decoupled from both the NBL and the free atmosphere, remaining a mixed layer during the night. In this structure, $NO_3\bullet$ and N_2O_5 may remain reactive and are retained in the decoupled RL in the absence of solar radiation (Brown et al., 2016; Chang et al., 2011).

Many modeling and measurement studies have examined the vertical distributions of nighttime N_2O_5-related chemical species. Although modeling studies have indicated strong vertical gradients of NO_3^- and N_2O_5 above the NBL (Fish et al., 1999; Galmarini et al., 1997; Geyer and Stutz, 2004; Riemer et al., 2003), their features at different altitudes have been reported to vary regionally. In measurement studies, broadband lidar measurements have shown that the total column abundance of NO_3^- is several hundred ppt_v, which is well in excess of typical surface-level nitrate mixing ratios (Povey et al., 1998) and indicative of reactions among N_2O_5-related chemical species in the upper atmosphere. Thus, both approaches imply that nighttime N_2O_5 can act as a reservoir of NO_x and O_3 aloft, and that this reservoir is related to the RL and therefore to the concentration of PM aloft. In the morning and daytime hours of the following day, N_2O_5 and $NO_3\bullet$ may influence the surface level during the development of the convective daytime ABL. This influence occurs during periods of intense vertical mixing or when local circulations such as mountain breezes are prevalent (Yun et al., 2024).

Nevertheless, nighttime N_2O_5 chemistry in the upper atmosphere is generally poorly understood, due to the absence of comprehensive measurements of N_2O_5-related chemical species, including over the SMA and northeast Asia. In this study, we conducted simulations using the Weather Research and Forecasting-Community Multiscale Air Quality (WRF-CMAQ) model, targeting nighttime vertical profiles of N_2O_5-related chemical species including NO, NO_2, and NO_3^- to gain a better understanding of nighttime conversion to NO_3^- over the Korean Peninsula. A heavy $PM_{2.5}$ winter episode during March 16–17, 2016 was selected as the study period based on a previous study, which showed that elevated PM was induced by nighttime heterogeneous reactions of N_2O_5 (Jo et al., 2022).

In addition, we conducted the same modeling study for the KORUS-AQ campaign cases, and analyzed the vertical distribution characteristics of N_2O_5-related species at night over the SMA. In our simulation of nighttime N_2O_5 chemistry for several cases, we particularly characterized the vertical distribution of N_2O_5-related species in association with NBL and RL structures. Despite the high uncertainties of our analysis, its results provide important reference data on the vertical distribution of N_2O_5-relevant chemical species over the SMA and will contribute to aircraft-based campaigns investigating high-PM plumes and high levels N_2O_5-related chemical species at high altitudes over the Korean Peninsula.

2. Methods and data

2.1. *N_2O_5 heterogeneous chemistry*

The chemical reactions related to NO_3^- formation via N_2O_5 heterogeneous chemistry and to the formation of particulate NO_3^- are shown in Reactions (1)–(6):

$$NO_{2(g)} + O_{3(g)} \rightarrow NO_3\bullet_{(g)} + O_{2(g)} \quad \text{(R1)}$$

$$NO_3\bullet_{(g)} + NO_{2(g)} \rightarrow N_2O_{5(g)} \quad \text{(R2)}$$

$$N_2O_{5(g)} \rightarrow NO_3\bullet_{(g)} + NO_{2(g)} \quad \text{(R3)}$$

$$N_2O_{5(g)} + H_2O_{(het)} \rightarrow 2HNO_{3(aq)} \quad \text{(R4)}$$

$$N_2O_{5(g)} + Cl^-_{(het)} \rightarrow Y\cdot ClNO_{2(g)} + (2\text{-}Y)\cdot HNO_{3(aq)} \quad \text{(R5)}$$

$$HNO_{3(g)} + NH_{3(g)} \rightarrow NH_4NO_{3(s)} \quad \text{(R6)}$$

During the day, $NO_3\bullet$ is formed via (R1) at very low rates due to high NO emissions, which titrate O_3, thereby altering the relative amounts of NO_2 and O_3 but conserving odd oxygen ($O_x \equiv NO_2 + O_3$). Nighttime $NO_3\bullet$ is formed via the reaction of NO_2 with O_3 (R1), with N_2O_5 generated via (R2), and N_2O_5 dissociates back to $NO_3\bullet$ and NO_2 (R3). N_2O_5 heterogeneously reacts on aerosol surfaces and forms HNO_3 via (R4) or (R5), and produces NH_4NO_3 via reaction (R6). Reaction (R5) where N_2O_5 reacts with chloride ions (Cl^-) to form nitryl chloride ($ClNO_2$), was not considered in this study due to the lack of information on Cl^- concentrations and emissions during the study period. Instead, we assumed an HNO_3 yield of 2 in (R5) instead of (2-Y), where Y is the $ClNO_2$ yield. This assumption may lead to higher nitrate production, potentially causing nitrate overestimation during the study period. The heterogeneous hydrolysis of N_2O_5 (R4) is a major loss pathway for NO_x at night but produces NO_3^- aerosols that contribute to $PM_{2.5}$ via (R4)–(R6). N_2O_5 uptake via (R4) describes the condition under which the collision of N_2O_5 molecules with a PM produces chemical reaction products.

However, at night, $NO_3\bullet$ may be produced via (R1) under low NO_x conditions associated with the NBL-decoupled RL. These reactions play important roles in determining the vertical profiles of nighttime N_2O_5-related chemical species such as $NO_3\bullet$ and N_2O_5. Fig. 1 provides a simplified illustration of N_2O_5 chemistry and the decoupled RL structure.

2.2. *Cases selection and modeling system*

Over the SMA, stagnant atmospheric conditions typically reflect a stagnant or slowly moving anticyclone system accompanied by weak horizontal and vertical mixing (Kim et al., 2018; Park et al., 2005). Under atmospherically stagnant conditions, such as those occurring on relatively dry early spring days, local emissions primarily support high $PM_{2.5}$ concentrations through the accumulation of air pollutants. Therefore, it is advisable to select cases with stagnant meteorological conditions to examine the impact of local heterogeneous conversion of N_2O_5 to HNO_3 on NO_3^- and $PM_{2.5}$ concentrations.

As an example of stagnant case, previous study modeled the case for

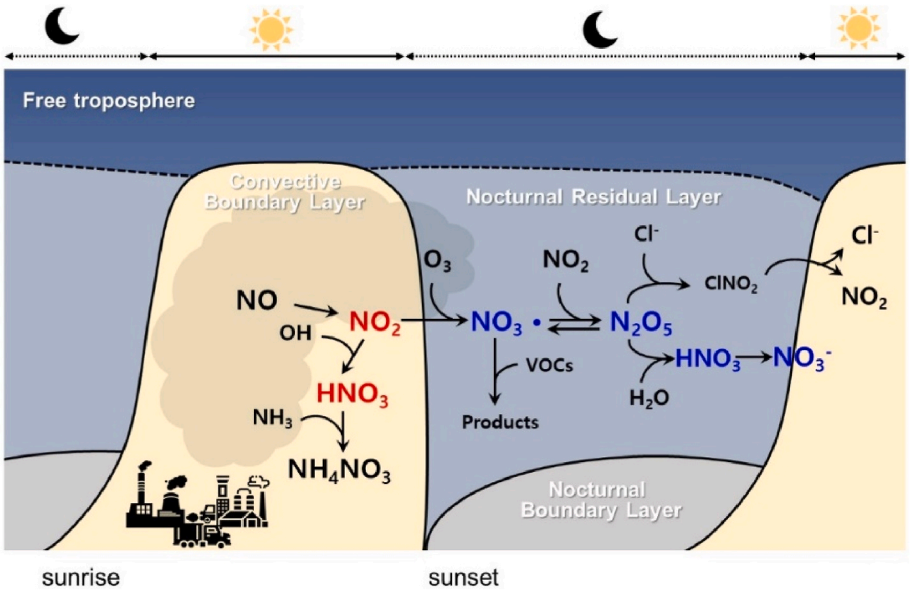

Fig. 1. Schematic illustration of nighttime heterogeneous dinitrogen pentoxide (N_2O_5) chemistry and secondary nitrate (NO_3^-) formation.

March 16–17, 2016, with data interpretation considering the dominance of secondary NO_3^- particle formation in nighttime N_2O_5 chemistry (Jo et al., 2019). Detailed information on the stagnant-dominated meteorological conditions is provided by Jo et al. (2019). We confirmed that the study periods—March 16–17, 2016—can be also classified as stagnant periods according to another classification method by Jo and Kim (2013). Therefore, concentration changes due to transboundary effects were expected to be minimal during the period.

For modeling, the WRF-CMAQ regional air quality model was employed. The WRF-CMAQ model configurations for meteorology, as well as gas and aerosol characteristics, are listed in Table S1. In the CMAQ configurations, the SAPRC99 gas-phase mechanism and the AERO5 aerosol modules with ISORROPIA-II for aerosol thermodynamics were selected for the gas-phase and aerosol-phase chemistry, respectively (Table S1).

The simulation domain, consisting of three nested domains, is shown in Fig. 2. Vertical layers are configured into a total of 31 layers; the lower atmospheric layers within approximately 1 km consist of 7 layers, with the sigma value of the lowest layer set at 0.9965, and the top layer is at 50 hPa. The meteorological initial and boundary conditions for WRF-CMAQ were obtained from the UK Met Office Unified Model global forecasts operated by the Korean Meteorological Administration (KMA) with a spatial resolution of ~25 km and a temporal resolution of 3 h. A week-long (seven-day) period was applied for spin-up. Vertically, and there were 15 layers on a sigma coordinate up to 50 kPa with the lowest layer thickness of about 32 m. Anthropogenic emissions for Northeast Asia are based on the Intercontinental Chemical Transport Experiment-Phase B (INTEX-B) inventory for the year 2006 (Li et al., 2014; Zhang et al., 2009), and the Clean Air Policy Support System (CAPSS) inventory for the year 2007 was used for Korea. Biogenic emissions considered here are based on the Model of Emissions of Gases and Aerosols from Nature (MEGAN) version 2.04.

2.3. Parameterization of N_2O_5 heterogeneous uptake coefficients

In the CMAQ (v.5.0.2), the N_2O_5 uptake coefficient (γN_2O_5) was

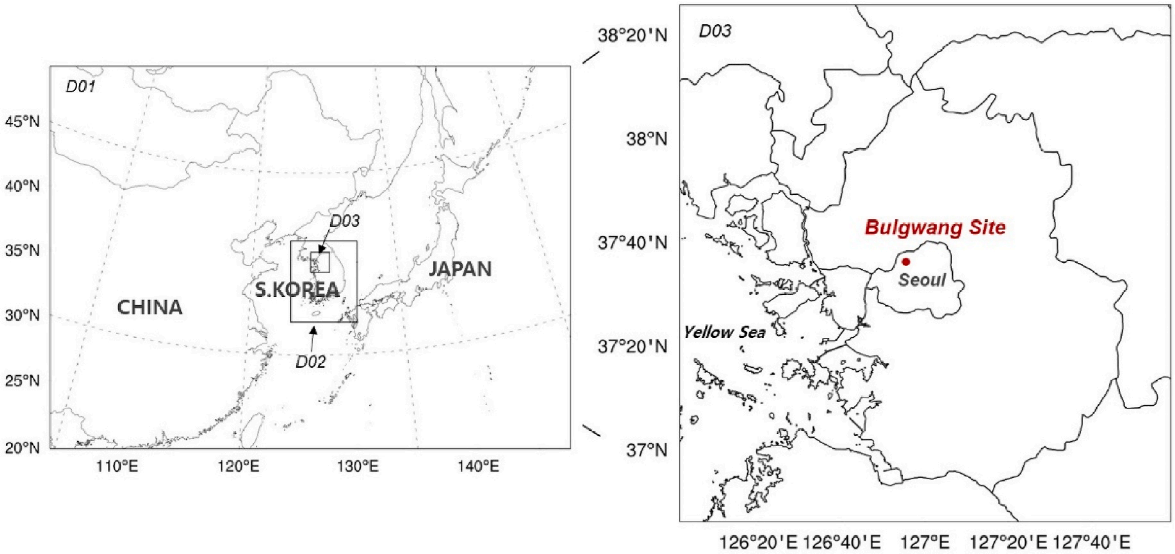

Fig. 2. Modeling domains D01, D02, and D03, with 27-, 9- and 3-km grid resolution, respectively, over the Seoul Metropolitan Area (SMA). Red dot indicates the Bulgwang site, where ground measurements were conducted.

parameterized as a function of particle composition and meteorological factors. Davis et al. (2008) developed a parameterization for γN_2O_5, incorporating factors such as temperature (T), relative humidity (RH), particle composition (including $(NH_4)_2SO_4$, and NH_4NO_3), and phase state (such as dry particle or aqueous particle) for application in air quality models. Their approach was based on an extensive dataset, which included all available measurements relevant to the γN_2O_5 on $(NH_4)_2SO_4$ and NH_4NO_3, derived from seven independent laboratory studies (Davis et al., 2008; McDuffie et al., 2018a, 2018b). The resulting equations were formulated as non-linear functions of RH and T.

$$\gamma N_2O_5 = f\,(RH, T, \text{sulfate-nitrate-ammonium conditions, phase state}, \ldots)$$

This parameterization demonstrated strong performance, accurately predicting 80% of the laboratory data within a factor of two and 63% within a factor of 1.5. More detailed descriptions of γN_2O_5 can be found in Davis et al. (2008).

2.4. Data

The chemical and meteorological WRF-CMAQ simulation results were evaluated based on *in situ* ground measurements obtained at the Bulgwang supersite located in the central SMA (Fig. 2). Various measurements relevant to $PM_{2.5}$ chemical components are conducted at the Bulgwang supersite, which has been operating by the National Institute of Environmental Research (NIER). For model verification and interpretation, simulated mass concentrations of chemical components including NO_3^-, SO_4^{2-}, NH_4^+, and $PM_{2.5}$ were compared with measured values. Simulated meteorological variables were also verified in comparison with meteorological observations provided by the KMA.

3. Results and discussion

3.1. Meteorological variables

Simulated and observed meteorological variables such as temperature at a height of 2 m (T2), RH, wind speed (WS), and direction (WD) at a height of 10 m at Bulkwang throughout the study period are shown in Fig. S1. Model performance was verified against observations from KMA based on indexes of agreement (IOA) for T2, RH, and WS, which were 0.93, 0.87, and 0.68, respectively (Fig. S1). These values indicate that the simulation results are in good agreement with observed data, with no significant biases in terms of both temporal patterns and amplitudes. In most mesoscale modeling cases, WS tends to be overestimated at night due to the impact of coarse surface conditions and boundary layer parameterization on weather forecasting (Kim et al., 2021), but the current modeling results are found to closely match the observed wind speed during the study period (Fig. S1), making it very suitable for simulating and analyzing nocturnal heterogeneous N_2O_5-chemistry. In particular, during the night, the observed lower wind speeds were simulated such that the weak turbulence conditions were expected to favor the accumulation of PM pollution associated with N_2O_5 chemistry.

3.2. Chemical variables

Fig. 3 shows the surface concentrations of several chemical variables ($PM_{2.5}$, NO_3^-, SO_4^{2-}, and NH_4^+) measured and simulated at the Bulgwang site throughout the study period. In Fig. 3, the model underestimated the daily mean concentrations of $PM_{2.5}$ and NO_3^- after 1200 KST on March 16, 2016. However, both the model and observations show morning and evening peaks of $PM_{2.5}$ and NO_3^- throughout the entire study period.

The observed chemical content of $PM_{2.5}$ during the study period was 40.5 ± 5.7 μg/m^3, and the sum of the three components NO_3^-, SO_4^{2-}, and $NH4^+$ was 26.1 ± 4.2 μg/m^3, accounting for 64.4% of the mass concentration of $PM_{2.5}$ (Fig. 3). Among these three components, NO_3^- was the major inorganic ion by mass, with an average ratio of NO_3^- to $PM_{2.5}$ of 0.28, which was approximately triple that of the SO_4^{2-} ratio (0.11) and twice that of the NH_4^+ ratio (0.15). Similar temporal variations in $PM_{2.5}$ and NO_3^- concentrations during the study period were observed; specifically, the times of peak concentrations for the two species differed by only 1–2 h, while the times of lowest concentrations matched exactly.

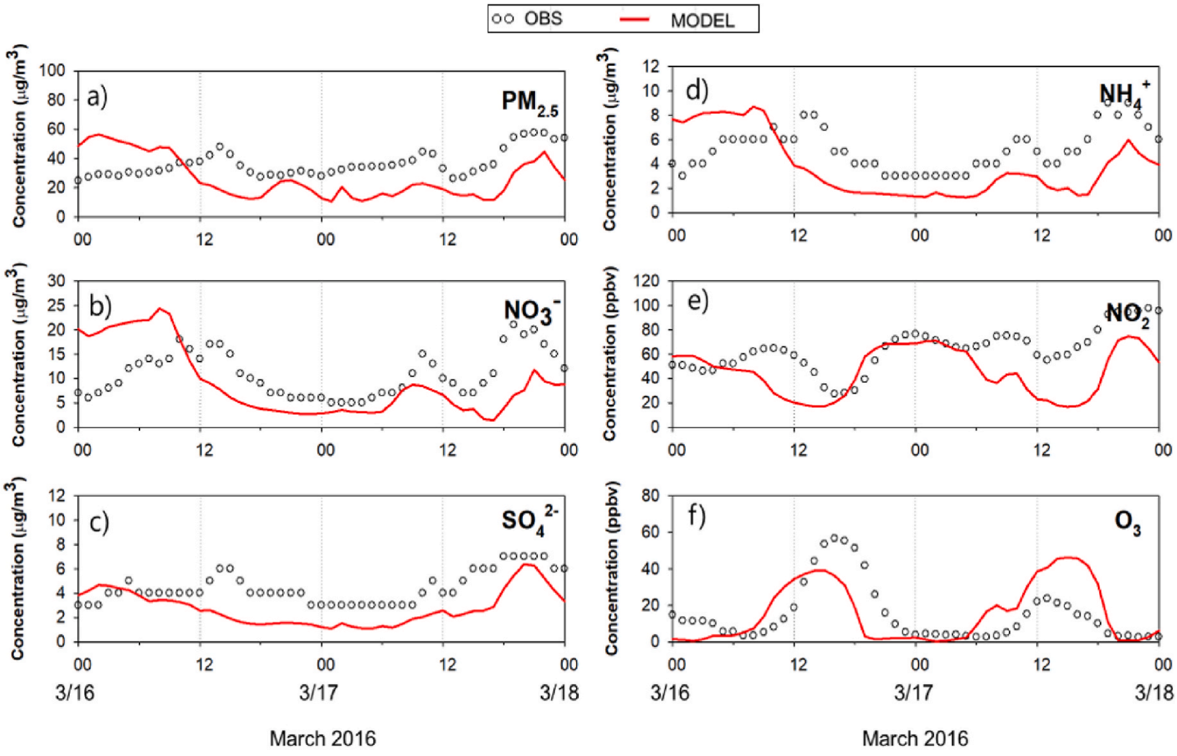

Fig. 3. Observed and simulated (a) $PM_{2.5}$ mass, (b) NO_3^-, (c) SO_4^{2-}, (d) NH_4^+, (e) NO_2, and (f) O_3 concentrations at the Bulgwang site in the SMA.

This provides further evidence that NO_3^- was the major chemical component in $PM_{2.5}$. All statistical parameters for model evaluation, such as IOA, normalized mean bias (NMB), and correlation coefficient (R), which represent the uncertainty levels of the model, are presented in Table S2. The modeled $PM_{2.5}$ and sulfate-nitrate-ammonium (SNA) concentrations are slightly underestimated, with the exception of the period prior to 1200 KST on March 16, 2016.

Despite the uncertainty in heterogeneous NO_3^- formation during the study period, the average observed nighttime NO_3^- concentration accounted for 31% of the $PM_{2.5}$ composition, whereas nighttime SO_4^{2-} and NH_4^+ together accounted for 22%. The simulated nighttime NO_3^- concentration also indicated the nighttime dominance of NO_3^-, with underestimations of SO_4^{2-} and NH_4^+. More detailed comparisons of ground-based measurements versus WRF-CMAQ modeling results can be found in Jo et al. (2019).

3.3. *Vertical structures of simulated NO_x, NO_3, O_3, and N_2O_5*

Fig. 4 shows the simulation of vertical distributions of NO_3^- and O_3, together with variations in ABL height at 6-h intervals from 0600 to 0000 KST. Trends in the vertical distribution of NO_3^- on March 16, 2016 were attributable to ABL variation for both day and night. The vertical profiles of NO_3^- particles during the daytime in March 2016 tended to be uniform within the ABL height at 1200 and 1800 KST (Fig. 4c and d), such that daytime concentrations were likely governed by strong vertical mixing induced by ABL dynamics. Notable N_2O_5 heterogeneous chemistry was simulated from the evening of March 16 to the early morning of March 17, 2016. On the night of March 16–17, surface NO_3^- levels remained high (+3.0–8.0 μg/m^3) (Fig. 4e and f), presumably due to NBL activity. Thus, the NBL acted as a lid on NO_3^-, constraining pollutants to within the shallow NBL height. The secondary peak of NO_3^- was simulated at around 500 m at 0600 KST on March 17 (Fig. 5f), which likely accounted for the increased NO_3^- concentration at 1200 and 1800 KST on the same day (Fig. 5g and h). Daytime surface O_3 levels ranged from 15 to 35 ppb on March 16–17 (i.e., Fig. 4c–g). However, in the upper atmosphere, higher levels of O_3, up to 60 ppb, were simulated for both day and night. Throughout the study period, daytime and nighttime O_3 concentrations were lower in the lower atmosphere and higher in the upper atmosphere (Fig. 4).

Fig. 5 shows the simulated vertical distributions of N_2O_5 and $NO_3\bullet$ concentrations throughout the study period. At 0600, 1200, 1800, and 0000 KST, both distributions were influenced by ABL height variation. Similar to NO_3^-, vertical mixing of N_2O_5 and $NO_3\bullet$ followed similar patterns within the ABL during daytime (Fig. 5c, d, g, h). However, at night, there was a clear difference in the altitude where the peak appeared; thus, nighttime peak values of $NO_3\bullet$ occurred at heights of 700–800 m, whereas those of N_2O_5 occurred at heights of 300–400 m (Fig. 5e and f). These altitude differences were due mainly to the heterogeneous nocturnal N_2O_5 chemistry associated with the decoupled RL.

Fig. S2 shows the time series of the vertical structures of NO, NO_2, O_3, $NO_3\bullet$, N_2O_5, and NO_3^-, along with the time series of RL, while Fig. 6 illustrates the interactions of chemical reactions of N_2O_5-related chemical species at the Bulkwang site. In this study, the RL height was defined as the simulated ABL height at the time of sunset. In Fig. 6 and Fig. S2, well-established daytime photochemical interactions occurred between NO_2, volatile organic compounds, and O_3; therefore, NO_2 concentrations were relatively low but retained a uniform vertical distribution influenced by strong vertical mixing within the ABL. At night, a shallow but stable NBL resulted in poor vertical mixing, leading to the accumulation of NO_2 at the surface and in turn to the simulation of higher nighttime

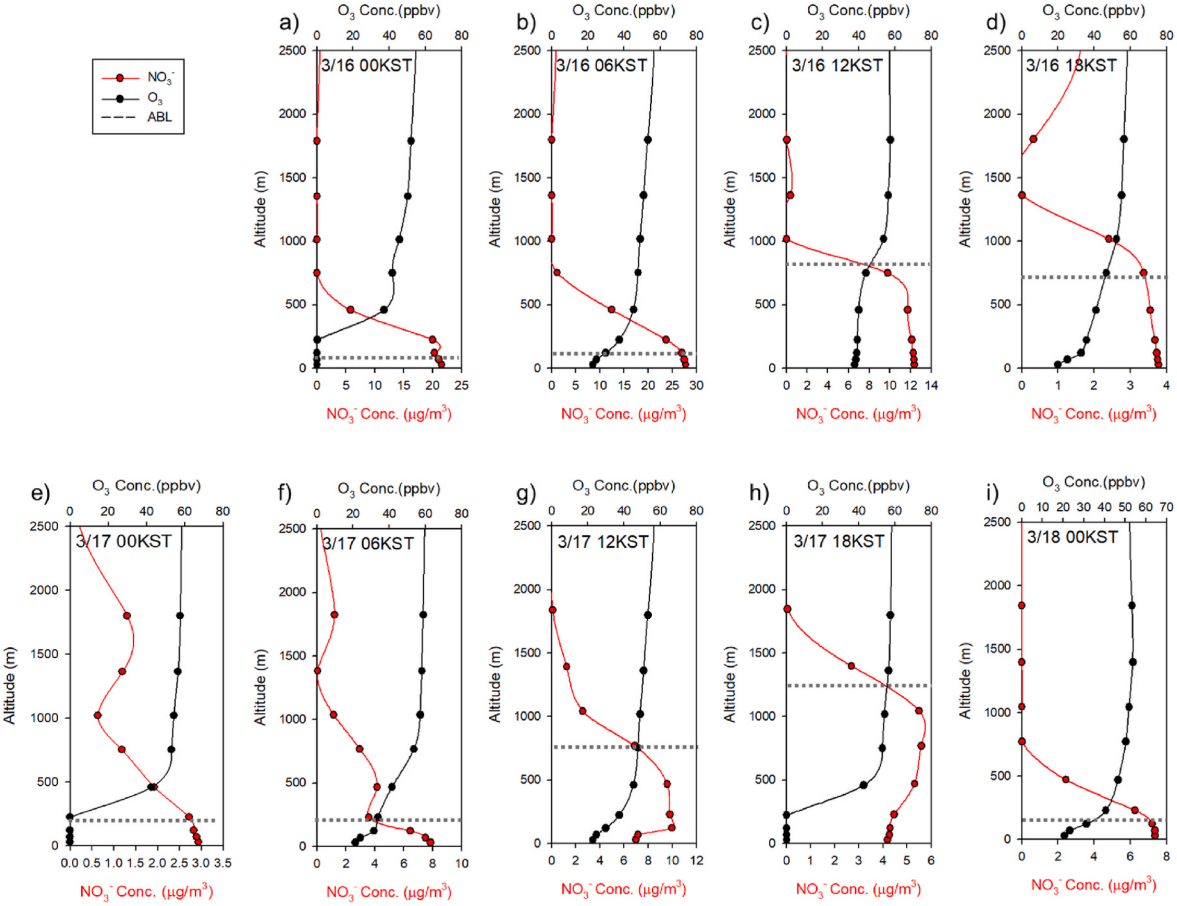

Fig. 4. Simulated vertical profiles of NO_3^- and O_3 at the Bulkwang site in the SMA. Dot lines indicate atmospheric boundary layer (ABL) heights.

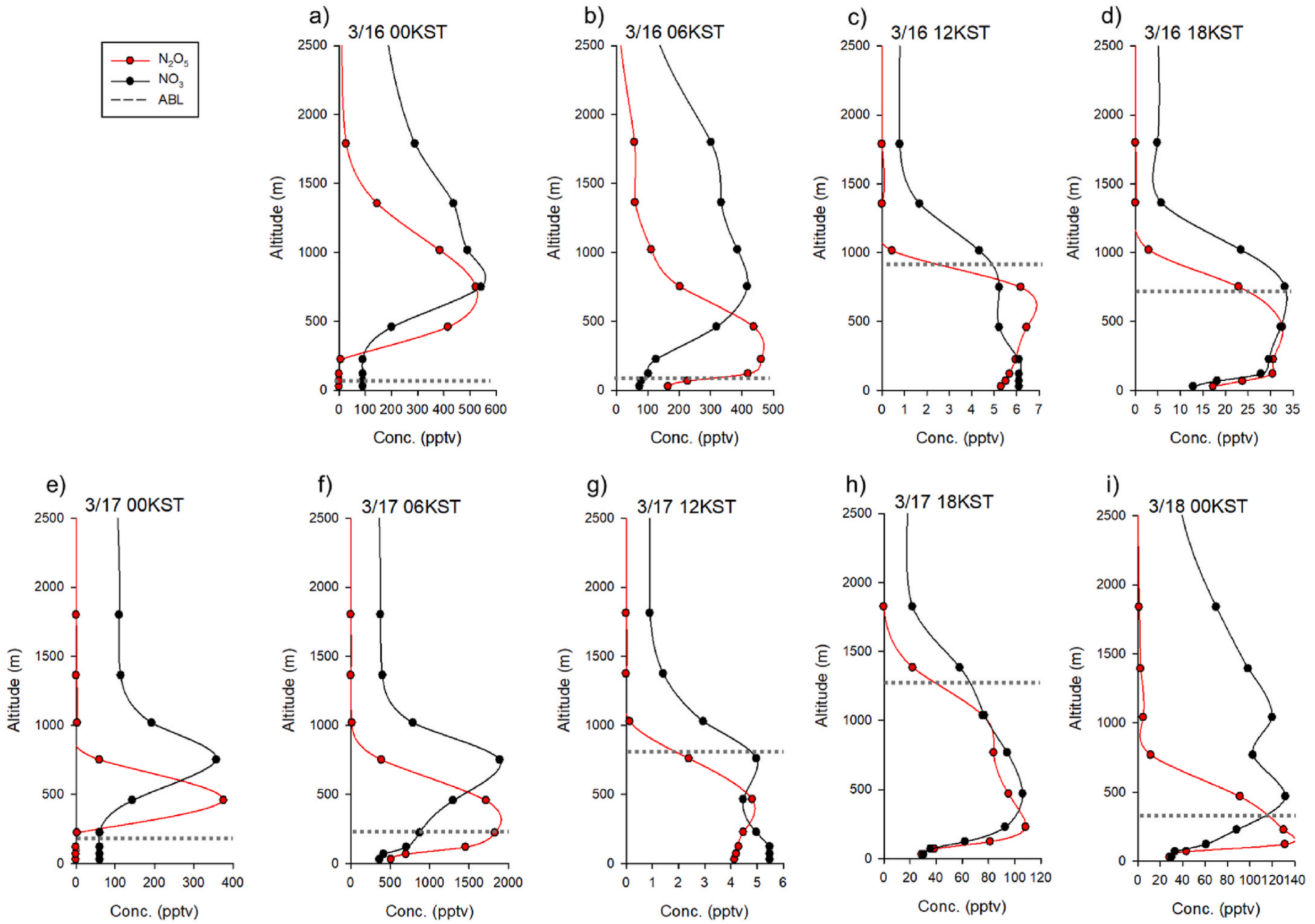

Fig. 5. Simulated vertical profiles of NO_3· and N_2O_5 at the Bulkwang site in the SMA. Dot lines indicate atmospheric boundary layer (ABL) heights.

surface NO_2 concentrations. Nocturnal NO_x titration decreased the amount of O_3, promoted by the high NO_x concentration at the surface under atmospheric conditions in the absence of sunlight; the resulting scarcity of surface O_3 hindered the production of NO_3• via (R1) in the near-surface atmosphere (Fig. 6).

However, unlike surface O_3, higher O_3 concentrations (up to 60 ppb) were simulated in the upper atmosphere, as also shown in Fig. 4. The simulated O_3 levels, which exceeded 50 ppb at altitudes above 1 km (Fig. 6), were also consistent with the results of the KORUS–AQ campaign (Lee et al., 2020). The decline in simulated NO_2 concentrations at altitudes of ≥300 m created an excess of O_3 compared with NO_2, which favored the generation of NO_3• via (R1) (Pusede et al., 2016). A peak in NO_3• occurred at 500–800 m, consistent with the results shown in Fig. 6, whereas N_2O_5, generated via (R2), peaked at an altitude of 200–600 m, which was lower than the peak of NO_3• generation (Fig. 6 and Fig. S2). Regarding nighttime N_2O_5 chemistry, NO_3• production was very low under NO_x-rich conditions due to high NO_x emissions and their resultant vigorous titration effect, particularly at ground level. However, NO_3• generation simulated in the current study remained active in the ground-decoupled RL at ~500–800 m altitude, with a peak at ~700 m (Fig. 6). The N_2O_5 peak was observed at ~300–400 m in the RL, which was lower than the NO_3• peak. This difference was due to the formation of N_2O_5 via (R2), which involved NO_2 and accordingly occurred at lower altitudes.

3.4. *Temporal evolution of vertical structures in accordance with chemical reactions*

Given the nighttime production of NO_3• in the decoupled RL, N_2O_5 was formed via (R1)–(R2), with the formation of NO_3^- in the RL through N_2O_5 uptake (R4). Following N_2O_5 generation, its uptake became highly significant for NO_3^- formation. Our study indicated that N_2O_5 aloft in the RL at ~200–600 m is maintained via (R1) and (R2), through the activity of NO_3• within the RL. Initially, heterogeneous N_2O_5 uptake (loss rate of N_2O_5) was a function of the total aerosol surface area and the fraction of gas–particle collisions, leading to the secondary formation of NO_3^-. This uptake process has been addressed in previous studies (Brown et al., 2016; Chang et al., 2011), and its sensitivity was tested using uptake coefficients in several studies (i.e., Jo et al., 2019).

In Fig. 6, the time series of N_2O_5 chemical reactions effectively illustrates the chemical interactions among the species. During NO_3• formation via $NO_2 + O_3 \rightarrow NO_3$• (R1), vertical profiles of nighttime surface NO_2 accumulation were well simulated, whereas nighttime O_3 increased vertically with increasing altitude (Fig. 6). Normally, the surface NO_3• concentration is zero; however, because NO_3• was active in the RL, N_2O_5 acted as a reactive intermediate to form HNO_3 and NO_3^-. In our simulation, excessive O_3 compared with NO_2 yielded NO_3• via reaction (R1), with the maximum level occurring at ~700 m in the RL (Fig. 6). NO_3• can be trapped and remain active with no sinks within the decoupled RL, such that it reacts with NO_2 via (R2), forming N_2O_5, with a maximum occurring at ~200–600 m in this study (Fig. 6).

N_2O_5 loss was caused by the uptake by aerosols via (R3)–(R6), whereupon N_2O_5 reacted with aerosol-phase water to yield HNO_3 (R4)

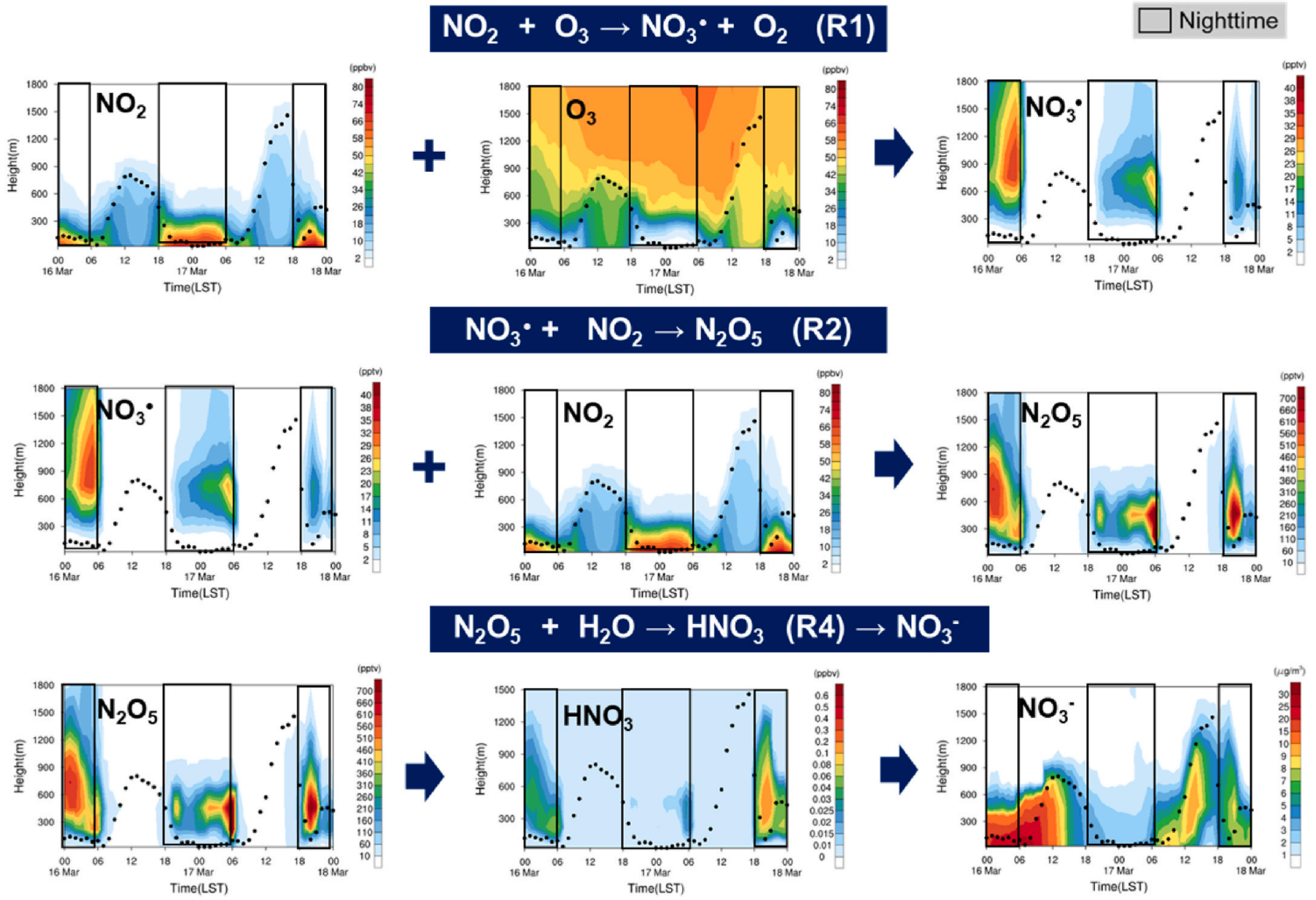

Fig. 6. Simulated time series of the vertical profiles of N_2O_5-related chemical species during sequential chemical reactions at the Bulgwang site. The rectangula box areas represent nighttime periods.

and, secondarily, NO_3^- via (R6). The homogeneous formation of HNO_3 from N_2O_5 (g) + H_2O (g) (R4) occurred during the nighttime formation of NO_3^-, but proceeded more slowly than the heterogeneous formation of HNO_3 through the heterogeneous hydrolysis of N_2O_5 on or within aqueous aerosol particles (Phillips et al., 2016; Ren et al., 2006; Wahner et al., 1998). As a final step, the formation processes resulting from both homogeneous and heterogeneous reactions yielded NH_4NO_3 particles via (R4)–(R6).

Even in situations where low concentrations of HNO_3 or NO_3^- are maintained at the surface (Figs. 3 and 6), high concentrations of N_2O_5 persist in the upper atmosphere during the nighttime RL on March 16, the night of March 16–17, and until 00:00 KST on March 18. Furthermore, it can be confirmed that the N_2O_5 chemical reactions progress towards HNO_3 or NO_3^- (Fig. 6). However, as shown in Fig. 6, for the 200–600 m range, the reaction rate of the (R4)–(R6) was relatively slower during the night of March 16–17 compared to the periods from 0000 to 0600 KST on March 16 and from 1800 KST on March 17 to 0000 KST on March 18. This difference could potentially be attributed to various factors, such as the variation in γN_2O_5 or other physical/chemical factors during the night.

To further investigate the cause, several N_2O_5-related variables at the 200–600 m range were examined. Fig. 7 shows the vertical distributions of γN_2O_5, and RH simulated by the WRF-CMAQ model at 6-h time intervals. The vertical profile of T is presented in Fig. S3, and the vertical variation in T was simulated to be minimal (see Fig. S3). Furthermore, under extremely low RH conditions, it has been reported that the γN_2O_5 value is almost independent of temperature (Davis et al., 2008). In this study, the correlation of γN_2O_5 with RH was also found to be the most significant. As shown in Fig. 7, the γN_2O_5 (×1000) during the night of March 16–17 was significantly low, ranging from 0.5 to 0.8, compared to the higher ranges of 4.8–21.6 for other nighttime hours, such as 0000 to 0600 KST on March 16, or 1800 KST on March 17 to 0000 KST on March 18. This low γN_2O_5 value is well associated with low RH (and relatively lower NO_3^-) during the night (Fig. 6). Due to the slow loss to the aerosol uptake process caused by significantly lower γN_2O_5 (Fig. 7), N_2O_5 remained trapped at high concentrations within the 200–600 m range until the early morning hours of March 17 (Fig. 6).

However, at 0000 KST on March 17, the γ N_2O_5 (×1000) values near the surface, where NO_3^- and RH were relatively higher, maintained levels of approximately 4.0–5.5, indicating a significant difference in the N_2O_5 uptake process rates between the upper and lower layers. This aligns with a prominent feature described by Davis et al. (2008), where γN_2O_5 is more sensitive to RH than to temperature under conditions where NH_4NO_3 dominate over $(NH_4)_2SO_4$ and the RH is below the deliquescence RH (DRH). Specifically, under significantly lower RH conditions (e.g., RH $<$ 20%), γN_2O_5 values decrease sharply with decreasing RH (Davis et al., 2008). Based on this understanding, the elevated nighttime N_2O_5 concentrations simulated in the 200–600 m range of the RL during the study period (e.g., near 0600 KST on March 17 in Fig. 6) were interpreted as the result of low γN_2O_5, primarily caused by low RH. Accordingly, the simulated HNO_3 and NO_3^- formed through N_2O_5 chemistry under extremely low RH conditions (8–18%), which led to elevated N_2O_5 concentrations remaining in the RL (200–600 m) during the early nighttime hours of March 17. Additionally, the relatively low RH (20–40%) during the study period has been reported as a limitation of the aerosol thermodynamics module

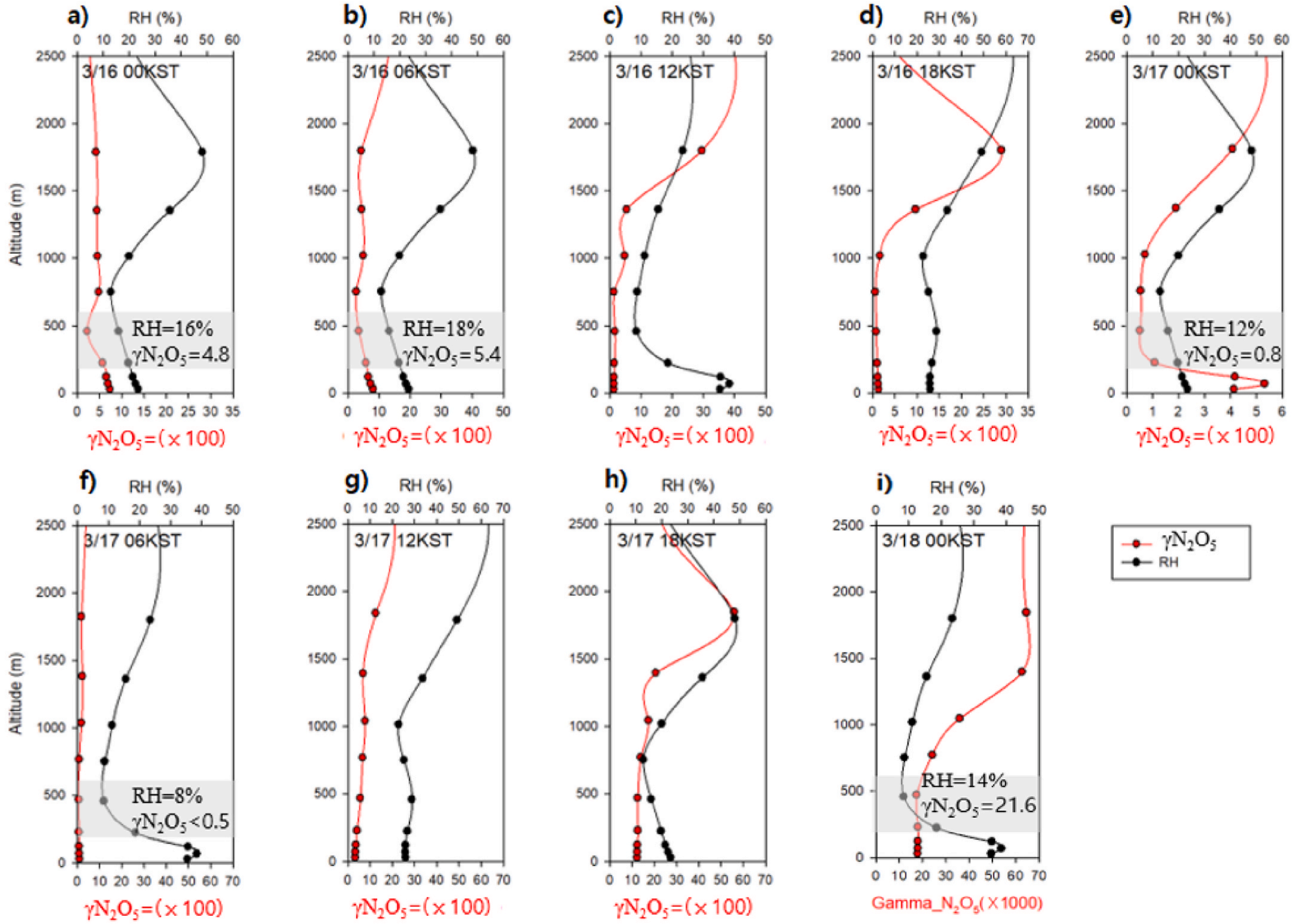

Fig. 7. Simulated vertical profiles of relative humidity (RH) and N_2O_5 uptake coefficient (γ N_2O_5) at the Bulkwang site in the SMA. The shaded areas indicate the altitude range of 200–600 m during the nighttime of March 16–17, 2016

ISORROPIA-II (Guo et al., 2016; Chang et al., 2016b), which was used in our WRF-CMAQ model. Therefore, it is essential to address these model uncertainties and conduct further parameterization studies on γN_2O_5 to improve the accuracy of the modeling study.

At sunrise of the following day, the primary product HO_x ($HO_x = OH + HO_2$) was activated through photochemical reactions, such that the daytime production rate of HNO_3 increased rapidly via the reaction $NO_2 + OH \rightarrow HNO_3$. In the previous study, the nighttime heterogeneous reaction of N_2O_5 was shown to drive nocturnal HNO_3 production, accounting for 50–90% of total nocturnal HNO_3, with the daytime production of HNO_3 activated by HO_x, accounting for 90% of total daytime HNO_3 (Seinfeld and Pandis, 1998). Combined with excess NH_3, the gas/particle partitioning of total (daytime + nighttime) HNO_3 will depend on the ambient temperature and humidity. Together, these results imply that NO_3^- can be actively formed during the early morning and daytime hours of the next day (Fig. 6), leading to high $PM_{2.5}$ events driven by high NO_3^- levels in urban areas.

3.5. Comparison with other field study: KORUS-AQ

In addition to the single case described above, we selected stagnant a multi-cases from the KORUS-AQ campaign period, and carried out the same analysis. Peterson et al. (2019) classified the KORUS-AQ campaign period (May 1– June 12, 2016) into four distinct synoptic conditions: dynamic meteorology (May 4–15), stagnant (May 16–22), transport (May 25–31), and blocking pattern (June 1–7) periods. We focused on the stagnation period (May 16–21) for this study. The modeling results for the KORUS-AQ campaign periods have been verified against surface measurements in several previous studies (Jo et al., 2023; Lee et al., 2020, 2023). However, there were few comparisons between non-surface aircraft measurements and modeling results. In this study, the aircraft measurements for the stagnation period (May 16–21, 2016) were used in model evaluation. Recalling that there were no flights at night during the KORUS-AQ campaign, we used daytime DC-8 measurements for model validation only in this study.

Fig. 8 illustrates the vertical profiles of NO_x, O_3, N_2O_5, and NO_3^- observed by the DC-8 aircraft over the SMA during May 16–21, 2016. Here, error bars represent one standard deviation. In Fig. 8, the vertical profiles of NO_x clearly demonstrate the influence of local emissions and photochemistry within the lowest 2 km, although the model results showed relatively lower levels compared to aircraft measurements. The simulated O_3 concentrations showed relatively lower compared to DC-8 measurements, with a particularly noticeable underestimation at altitudes above 2 km. Above 2–3 km, higher O_3 were observed, with an average value of approximately 80 ppb$_v$ and little vertical variation (NIER and NASA, 2017).

For N_2O_5, the DC-8 measurements revealed high variability up to ~2 km, with lower levels at the ground. However, consistent maximum N_2O_5 concentrations were observed around 1 km from the DC-8 measurements and around 700 m from the model simulations. NO_3^- exhibited higher concentrations at ground with high variability within 1 km, but secondary peaks were measured around 700 m from the DC-8

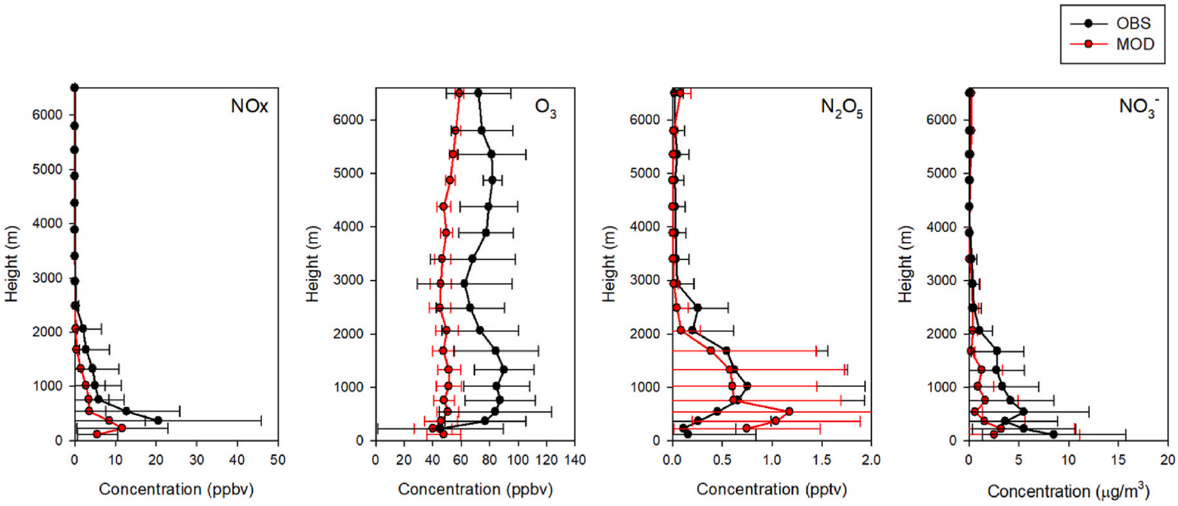

Fig. 8. Simulated and aircraft-measured vertical profiles of NO_x, O_3, N_2O_5, and NO_3^- concentrations over the SMA during the stagnant period of KORUS-AQ campaign (May 16–21, 2016).

and simulated around 800 m (Fig. 8). These results provide evidence for the role of nighttime heterogeneous N_2O_5-chemistry acting aloft, such as within the RL.

We performed WRF-CMAQ modeling for 6 days classified as stagnant weather conditions (May 16–21) during the KORUS-AQ campaign, and analyzed the vertical structures of N_2O_5-related species in the RL. Fig. S4 shows the vertical profiles of simulated NO, NO_2, O_3, NO_3•, N_2O_5, and NO_3^-, along with the RL height during May 16–21 at the Bulkwang site. Here, we found that, during the daytime, photochemical interactions led to relatively low and uniformly distributed NO_x (=NO + NO_2) concentrations (Fig. S4). At night, a NBL formed, resulting in the accumulation of NO_x, particularly NO_2, near the surface and a decrease in O_3 due to nocturnal NO_x titration, as observed during March 16–17 (also see Fig. 6). Likewise in Fig. 6, the decreasing vertical gradient of NO_2, combined with increasing O_3, facilitated the formation of NO_3•, with peaks at 700 m (May 16), 500 m (May 17), and 700–800 m (May 18,

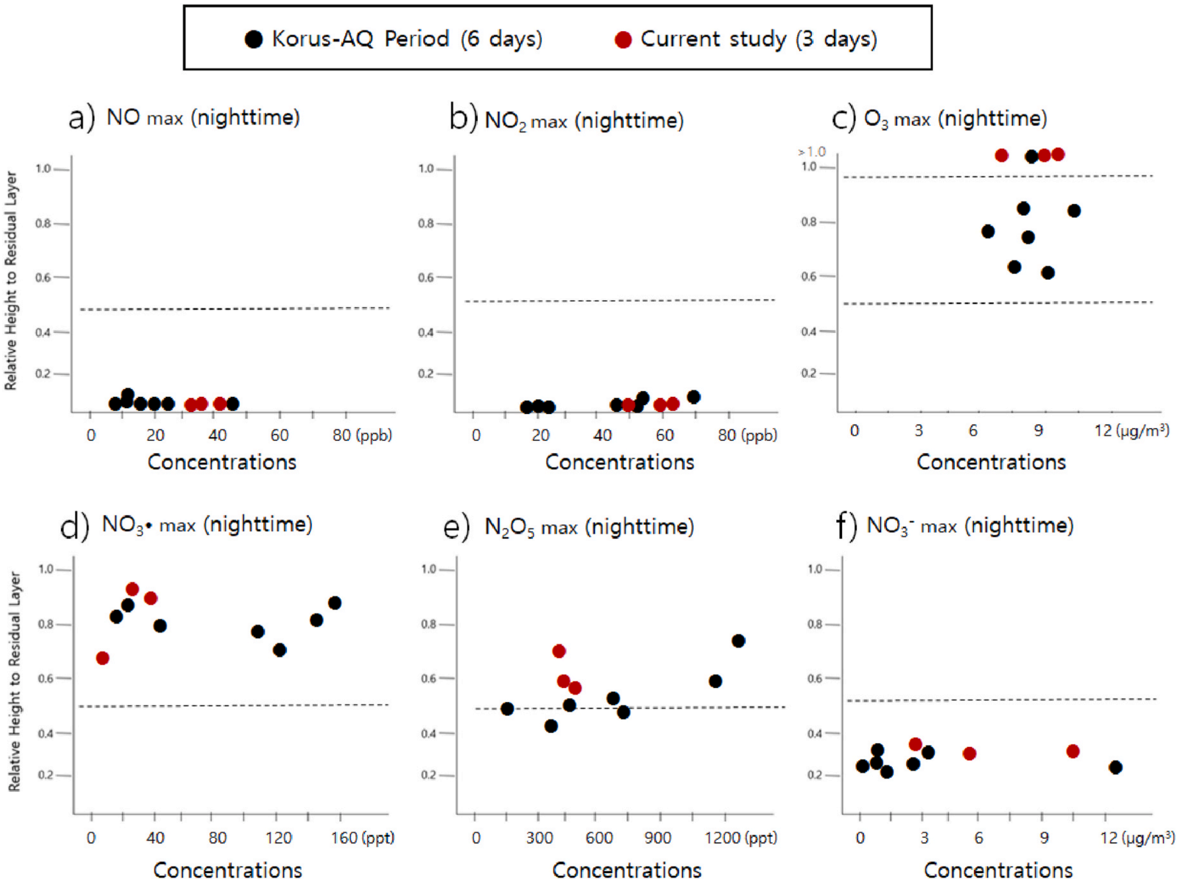

Fig. 9. Vertical distributions of the nighttime maximum concentrations of N_2O_5-related chemical species: (a) NO, (b) NO_2, (c) O_3, (d) NO_3•, (e) N_2O_5, and (f) NO_3^- during the periods of May 16–21, 2016 (KORUS-AQ campaign) and March 17–18, 2016.

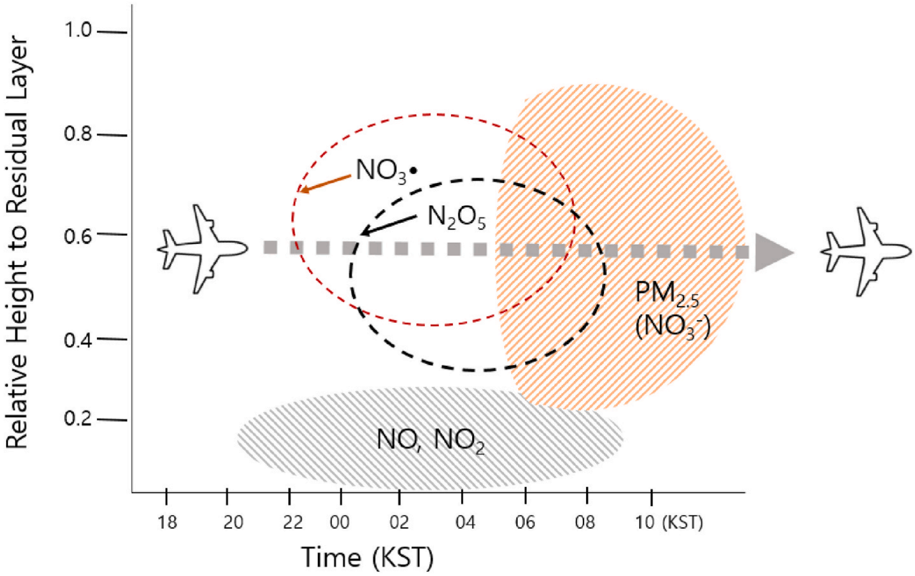

Fig. 10. Schematic illustration of the nighttime–height distributions of N_2O_5-related chemical species: NO, NO_2, NO_3·, N_2O_5, and NO_3^- over the SMA, as simulated by the WRF-CMAQ model. The y-axis is normalized to the residual layer (RL) height.

20–21), primarily through reaction (R1). The subsequent formation of N_2O_5, via reaction (R2) showed peaks at altitudes of 250–350 m (May 16), 350–500 m (May 17), and 850–1200 m (May 18), occurring lower than the NO_3• peak, which led to secondary formation of NO_3^- at the same altitudes. Comparable trends were noted on May 20–21. The NO_3^- concentrations increased a few hours after the N_2O_5 peak, around sunrise (see Fig. S4).

We tried to estimate the vertical altitudes of N_2O_5-related species relative to the RL height from KORUS-AQ and current study periods. Fig. 9 illustrates vertical distributions (relative to the RL height) of the nighttime maximum concentrations of N_2O_5-related species including NO, NO_2, O_3, NO_3•, N_2O_5, and NO_3^- for the stagnant cases during the KORUS-AQ campaign: May 16–21, 2016 (6-days) and the current study period: March 17–18, 2016 (3-days). In Fig. 9, NO and NO_2 levels all showed a maximum near the ground, while O_3 showed highest levels around RL height or more higher altitudes than RL. The peaks of maximum nighttime NO_3• and N_2O_5 concentrations were observed at 70–90% (78 ± 11%) and 40–70% (54 ± 13%) of the RL height, respectively. Again, these results clearly demonstrate that nighttime heterogeneous N_2O_5 chemical reactions occur more vigorously aloft, particularly within the RL, rather than near the surface atmosphere over the SMA.

Lastly, Cl-chemistry and its associated species such as the chlorine radical (Cl•) and $ClNO_2$ are involved in the nocturnal N_2O_5-chemistry and also in secondary NO_3^- formation pathways (Wang et al., 2019, 2020; Zhang et al., 2022). In (R5) $N_2O_5 + Cl^- \rightarrow Y{\cdot}ClNO_2 + (2\text{-}Y){\cdot}HNO_3$, $ClNO_2$ was not considered due to the unavailability of gridded Cl emission during the study period; we used HNO_3 yield of 2 in (R5) thus overestimation of nitrate particle was expected in this study. However, Cl-chemistry is particularly important because Cl^- reacts with N_2O_5 during the nighttime and forms $ClNO_2$, which is a critical factor in the formation of aerosol NO_3^- at high levels in NO_x-rich environments. By incorporating Cl emission and accounting for Cl-chemistry in this study, it would be possible to simulate more realistic to secondary NO_3^- formation.

Bertram and Thornton (2009) showed that $ClNO_2$ production reduced the total NO_3^- levels in the United States (by up to 0.8–2.0 μg/m^3 or 11–21%). However, there is a significant lack of modeling studies for the Northeast Asia region. Jo et al. (2023) conducted modeling study based on the latest anthropogenic Cl emissions (Zhang et al., 2022), and indicated that although addition of Cl emission did not significantly alter NO_3^- formation with the only minimal difference, although the differences in NO_3^- and NH_4^+ were not significant (<0.1 mg/m^3), the ability to simulate the $PM_{2.5}$ concentrations was slightly improved compared with the Cl emissions-free case. However, even in this case, only gridded anthropogenic Cl emissions were considered, while natural Cl emissions were not accounted for. In particular, given the geographical proximity of the Korean Peninsula to the Yellow Sea, the impact of gridded natural Cl emissions on modeling is significant. Therefore, it is urgent to establish the horizontal distribution of currently available natural Cl emissions.

3.6. Recommendations for aircraft field campaign

The altitudes at which high concentrations of various N_2O_5-related chemical species occurred were noteworthy. Our simulation of NO_3• and N_2O_5 formation aloft via the reactions (R1)–(R2) indicated that RL height is a crucial factor determining which altitudes are conducive to the formation of high levels of N_2O_5-related chemical species, and can also be used to determine optimal flight altitudes for aircraft-based atmospheric investigations.

Fig. 10 shows a time–height plot of N_2O_5-related chemical species, as determined from vertical profiles based on our modeling study. NO_x levels reached a maximum near the ground, whereas NO_3• maxima occurred at 0.7–0.8 times the RL height and N_2O_5 maxima at 0.4–0.7 times the RL height, respectively. These results are consistent with the dependency of N_2O_5 formation via (R2) on NO_2, which is more abundant at lower altitudes. The formation of both N_2O_5 and NO_3• is governed by the vertical structures of O_3 and NO_2 in the RL, and therefore by the NO_x emission rate and atmospheric stability of NO_x in the NBL and RL at night.

However, as the daytime convective boundary layer develops and the top of the next day's ABL reaches the base of the RL, NO_3^- formed at night can be mixed down toward the ground, adding to the accumulated surface NO_3^- levels. In summary, as the NBL develops with the RL above it, NO_3• remains within the RL, allowing N_2O_5 chemical reactions to occur. As the RL is not in direct contact with the ground, NO_3• and N_2O_5 are retained high aloft, and subsequently dispersed into the daytime mixed layer on the following day. Thus, RL height may be a crucial factor determining the optimal altitude for aircraft campaigns aimed at investigating N_2O_5 chemistry. In turn, the RL height is determined by the maximum daytime ABL height on the previous day.

4. Summary and conclusion

This study applied WRF-CMAQ modeling to simulate the vertical profiles of N_2O_5-related chemical species, which were then interpreted in association with RL development. The study period covered March 16–17, 2016, and also discussed for the period of KORUS-AQ campaign: May 16–22, 2016, during which measured NO_3^- concentrations indicated that nighttime heterogeneous N_2O_5 chemistry accounted for a large fraction of $PM_{2.5}$.

Our results showed that nighttime N_2O_5 heterogeneous chemistry can support the nighttime buildup of NO_3^-, and therefore that nocturnal NBL dynamics are a critical determinant of the altitudes of N_2O_5-related chemical species at night. Thus, according to our simulation results, as the NBL develops, overlain by the RL, NO_3• still resides in the decoupled RL, in contrast to the lack of NO_3• production at ground level. The simulated NO_3• peak occurred at 0.7–0.9 of the RL height, and the simulated N_2O_5 peak occurred at 0.4–0.7 of the RL height, which were lower than the NO_3• peak. The retention of these two species in the decoupled RL likely induced active N_2O_5 chemical reactions. Our results suggest that the relationship between the ABL or RL height and nighttime N_2O_5 heterogeneous chemistry contributed to the relative success of our simulation of the nighttime secondary formation of NO_3^- and ultimately of the $PM_{2.5}$ mass concentration.

Vertical profiles of N_2O_5-related chemical species over the SMA are lacking. However, our analysis of those profiles and the influence of the RL, although our study is based on modeling, provide crucial information on the optimal flight altitudes for aircraft measurement campaigns, such as SIJAC and ASIA-AQ campaigns. Nonetheless, our research covered only a limited study period, such that additional modeling of multiple cases and further verification of the results are needed for accurate estimates of the vertical structures of nighttime N_2O_5-related chemical species.

CRediT authorship contribution statement

Hyun-Young Jo: Writing – original draft, Formal analysis, Conceptualization. **Hyo-Jung Lee:** Validation, Software, Formal analysis. **Gookyoung Heo:** Methodology, Investigation, Conceptualization. **Cheol-Hee Kim:** Writing – review & editing, Funding acquisition, Conceptualization.

Declaration of competing interest

The authors declare that they have no known competing financial interests or personal relationships that could have appeared to influence the work reported in this paper.

Acknowledgements

This research was supported by the Basic Science Research Program through the National Research Foundation of Korea (NRF) funded by the Ministry of Education (2020R1A6A1A03044834 and 2020R1I1A1A01072998).

Appendix A. Supplementary data

Supplementary data to this article can be found online at https://doi.org/10.1016/j.atmosenv.2025.121119.

Data availability

Data will be made available on request.

References

Bertram, T.H., Thornton, J.A., 2009. Toward a general parameterization of N_2O_5 reactivity on aqueous particles: the competing effects of particle liquid water, nitrate and chloride. Atmos. Chem. Phys. 9, 8351–8363.

Brown, S.G., Roberts, P.T., McCarthy, M.C., Lurmann, F.W., 2006a. Wintertime vertical variations in particulate matter (PM) and precursor concentrations in the San Joaquin valley during the California regional coarse PM/Fine PM air quality study. J. Air Waste Manag. Assoc. 56 (9), 1267–1277.

Brown, S.S., Dubé, W.P., Tham, Y.J., Zha, Q., Xue, L., Poon, S., Wang, Z., Blake, D.R., Tsui, W., Parrish, D.D., Wang, T., 2016. Nighttime chemistry at a high altitude site above Hong Kong. J. Geophys. Res. 121, 2457–2475.

Brown, S.S., Ryerson, T.B., Wollny, A.G., Brock, C.A., Peltier, R., Sullivan, A.P., Weber, R. J., Dube, W.P., Trainer, M., Meagher, J.F., Fehsenfeld, F.C., Ravishankara, A.R., 2006b. Variability in nocturnal nitrogen oxide processing and its role in regional air quality. Science 311 (5757), 67–70.

Chang, L.-S., Kim, D., Hong, H., Kim, D.-R., Yu, J.-A., Lee, K., Lee, H., Kim, D., Hong, J., Jo, H.-Y., Kim, C.-H., 2022. Evaluation of correlated Pandora column NO2 and in situ surface NO_2 measurements during GMAP campaign. Atmos. Chem. Phys. 22, 10703–10720.

Chang, W.L., Bhave, P.V., Brown, S.S., Riemer, N., Stutz, J., Dabdub, D., 2011. Heterogeneous atmospheric chemistry, ambient measurements, and model calculations of N_2O_5: a review. Aerosol Sci. Technol. 45, 665–695.

Chang, W.L., Brown, S.S., Stutz, J., Middlebrook, A.M., Bahreini, R., Wagner, N.L., Dubé, W.P., Pollack, I.B., Ryerson, T.B., Riemer, N., 2016. Evaluating N_2O_5 heterogeneous hydrolysis parameterizations for CalNex 2010. J. Geophys. Res. Atmos. 121, 5051–5070.

Crawford, J.H., Ahn, J.-.Y., Al-Saadi, J., Chang, L., Emmons, L.K., Kim, J., Lee, G., Park, J.-H., Park, R.J., Woo, J.H., Song, C.-K., Hong, J.-H., Hong, Y.-D., Lefer, B.L., Lee, M., Lee, T., Kim, S., Min, K.-E., Yum, S.S., Shin, H.J., Kim, Y.-W., Choi, J.-S., Park, J.-S., Szykman, J.J., Long, R.W., Jordan, C.E., Simpson, L.J., Fried, A., Dibb, J. E., Cho, S., Kim, Y.P., 2021. The Korea-United States air quality (KORUS-AQ) field study. Elementa-Sci. Anthrop. 9 (1), 00163.

Davis, J.M., Bhave, P.M., Foley, K.M., 2008. Parameterization of N_2O_5 reaction prob abilities on the surface of particles containing ammonium, sulfate, and nitrate. Atmos. Chem. Phys. 8, 5295–5311.

Finlayson-Pitts, B.J., Pitts Jr., J.N., 2000. The vertical distribution of NO_3 in the atmospheric boundary layer. Atmos. Environ. 33, 687–691.

Fish, D.J., Shallcross, D.E., Jones, R.L., 1999. Chemistry of the Upper and Lower Atmosphere: Theory, Experiments, and Applications. Academic Press, San Diego, p. 969.

Galmarini, S., Duynkerke, P.G., DeArellano, I.V.G., 1997. Evolution of nitrogen oxide chemistry in the nocturnal boundary layer. J. Appl. Meteorol. 36, 943–957.

Geyer, A., Stutz, J., 2004. Vertical profiles of NO_3, N_2O_5, O_3, and NO_x in the nocturnal boundary layer: 2. Model studies on the altitude dependence of composition and chemistry. J. Geophys. Res. 109, D12307.

Guo, H., Sullivan, A.P., Campuzano-Jost, P., Schroder, J.C., Lopez-H, F.D., Dibb, J.E., Limenez, J.L., Thornton, J.A., Brown, S.S., Nenes, A., Webber, R.J., 2016. Fine particle pH and the partitioning of nitric acid during winter in the northeastern United States. J. Geophys. Res. Atmos. 121, 10355–10376.

Jo, H.-Y., Kim, C.-H., 2013. Identification of long-range transported haze phenomena and their meteorological features over Northeast Asia. J. Appl. Meteorol. Climatol. 52, 1318.

Jo, H.-Y., Lee, H.-J., Jo, Y.-J., Lee, J.-J., Ban, J.-L., Chang, L.-S., Heo, G., Kim, C.-H., 2019. Nocturnal fine particulate nitrate formation by N_2O_5 heterogeneous chemistry in Seoul Metropolitan Area, Korea. Atmos. Res. 225, 58–69.

Jo, H.-Y., Lee, H.-J., Jo, Y.-J., Heo, G., Lee, M., Kim, J.-A., Park, M.-S., Lee, T., Kim, S.-W., Lee, Y.-H., Kim, C.-H., 2022. A case study of heavy $PM_{2.5}$ secondary formation by N_2O_5 nocturnal chemistry in Seoul, Korea in January 2018: model performance and error analysis. Atmos. Res. 266, 105951.

Jo, H.-Y., Park, J., Heo, G., Lee, H.-J., Jeon, W., Kim, J.-M., Kim, S., Kim, J.-K., Liu, Y., Liu, P., Zhao, B., Kim, C.-H., 2023. Interpretation of the effects of anthropogenic chlorine on nitrate formation over northeast Asia during KORUS-AQ 2016. Sci. Total Environ. 894, 164920.

Kim, C.-H., Jo, H.-Y., Jo, H.-Y., Lee, H.-J., Kim, J.-M., Lee, N.-M., Jeong, S.-Y., Baek, S.-H., Park, M.-J., Chang, L.-S., Lee, J.-J., Song, C.-K., 2023. Synoptic meteorological conditions and contributing factors to air quality during the SIJAQ campaign. Atmos. Environ. 309, 119939.

Kim, C.-H., Meng, F., Kajino, M., Lim, J., Tang, W., Lee, J.-J., Kiriyama, Y., Woo, J.-H., Sato, K., Kitada, T., Minoura, H., Kim, J., Lee, K.-B., Roh, S., Jo, H.-Y., Jo, Y.-J., 2021. Comparative numerical study of $PM_{2.5}$ in exit-and-entrance areas associated with transboundary transport over China, Japan, and Korea. Atmosphere 12 (4), 469.

Kim, C.-H., Lee, H.-J., Kang, J.-E., Jo, H.-Y., Park, S.-Y., Jo, Y.-J., Lee, J.-J., Yang, G.-H., 2018. Meteorological overview and signatures of long-range transport processes during the MAPS-seoul 2015 campaign. Aerosol Air Qual. Res. 18, 2173–2184.

Kim, S., VandenBoer, T.C., Young, C.J., Riedel, T.P., Thornton, J.A., Swarthout, R., Sive, B., Lerner, B.M., Gilman, J.B., Warneke, C., Roberts, J.M., Guenther, A., Wagner, N.L., Dubé, W.P., Williams, E.J., Brown, S.S., 2014. The primary and recycling sources of OH during the NACHTT-2011 campaign. J. Geophys. Res. 119, 6886–6896.

Lee, H.-J., Jo, H.-Y., Kim, J.-M., Bak, J., Park, M.-S., Kim, J.-K., Jo, Y.-J., Kim, C.-H., 2023. Nocturnal boundary layer height uncertainty in particulate matter simulations during the KORUS-AQ campaign. Remote Sens. 15, 300.

Lee, H.-J., Jo, H.-Y., Park, S.-Y., Jo, Y.-J., Jeon, W., Ahn, J.-Y., Kim, C.-H., 2019. A case study of the transport/transformation of air pollutants over the Yellow Sea during the MAPS 2015 campaign. J. Geophys. Res. Atmos. 124, 6532–6553.

Lee, H.-J., Jo, Y.-J., Kim, S., Kim, D., Kim, J.-M., Choi, D., Jo, H.-Y., Bak, J., Park, S.-Y., Jeon, W., Kim, C.-H., 2022. Transboundary aerosol transport process and its impact on aerosol- radiation-cloud feedbacks in springtime over Northeast Asia. Sci. Rep. 12, 4870.

Lee, H.-J., Jo, H.-Y., Song, C.-K., Jo, Y.-J., Park, S.-Y., Kim, C.-H., 2020. Sensitivity of simulated $PM_{2.5}$ concentrations over Northeast Asia to different secondary organic aerosol modules during the KORUS-AQ campaign. Atmosphere 11, 1004.

Li, M., Zhang, Q., Streets, D.G., He, K.B., Cheng, Y.F., Emmons, L.K., Huo, H., Kang, S.C., Lu, Z., Shao, M., Su, H., Yu, X., Zhang, Y., 2014. Mapping Asian anthropogenic emissions of non-methane volatile organic compounds to multiple chemical me chanism. Atmos. Chem. Phys. 14 (11), 5617–5638.

Lu, Y., Zhu, B., Huang, Y., Shi, S., Wang, H., An, J., Yu, X., 2019. Vertical distributions of black carbon aerosols over rural areas of the Yangtze River Delta in winter. Sci. Total Environ. 661, 1–9.

McDuffie, E.E., Fibiger, D.L., Dube, W.P., Lopez-Hilfiker, F., Lee, B.H., Jaeglé, L., et al., 2018a. $ClNO_2$ yields from aircraft measurements during the 2015 WINTER campaign and critical evaluation of the current parameterization. J. Geophys. Res. Atmos. 123, 12994–13015.

McDuffie, E.E., Fibiger, D.L., Dube, W.P., Lopez-Hilfiker, F., Lee, B.H., Thornton, J.A., et al., 2018b. Heterogeneous N_2O_5 uptake during winter: aircraft measurements during the 2015 WINTER campaign and critical evaluation of current para meterizations. J. Geophys. Res. Atmos. 123, 4345–4372.

NIER and NASA, 2017. Rapid Science synthesis (RSSR) report. Available at: https://espo.nasa.gov/sites/default/files/documents/KORUS-AQ-RSSR.pdf.

Oh, H.R., Ho, C.H., Koo, Y.S., Baek, K.G., Yun, H.Y., Hur, S.K., Choi, D.-R., Jhun, J.-G., Shim, J.-S., 2020. Impact of Chinese air pollutants on a record-breaking PMs episode in South Korea for 11–15 January 2019. Atmos. Environ. 223, 117262.

Oh, S.-S., Lee, H.-J., Kim, M.-S., Park, M.-S., Kim, C.-H., 2024. Aerosol-heat flux interactions in the boundary layer during the SIJAQ campaign. Atmos. Environ. 319, 120306.

Park, I.-S., Choi, W.-J., Lee, T.-Y., Lee, S.-J., Han, J.-S., Kim, C.-H., 2005. Simulation of long-range transport of air pollutants over Northeast Asia using a comprehensive acid deposition model. Atmos. Environ. 39, 4075–4085.

Park, R.J., Oak, Y.J., Emmons, L.K., Kim, C.H., Pfister, G.G., Carmichael, G.R., Saide, P. E., Cho, S.Y., Kim, S., Woo, J.H., Crawford, J.H., Gaubert, B., Lee, H.-J., Park, S.-H., Jo, Y.-J., Gao, M., Tang, B., Stanier, C.O., Shin, S., Park, H., Bae, C., Kim, E., 2021. Multi-model intercomparisons of air quality simulations for the KORUS-AQ campaign. Elementa-Sci. Anthrop. 9, 00139.

Park, S.-Y., Kim, C.-H., 2021. Interpretation of aerosol effects on precipitation susceptibility in warm clouds inferred from satellite measurements and model evaluation over Northeast Asia. J. Atmos. Sci. 78 (6), 1947–1963.

Park, S.-Y., Lee, H.-J., Kang, J.-E., Lee, T., Kim, C.-H., 2018. Aerosol radiative effects on mesoscale cloud–precipitation variables over Northeast Asia during the MAPS-Seoul 2015 campaign. Atmos. Environ. 172, 109–123.

Peterson, D.A., Hyer, E.J., Han, S.-O., Crawford, J.H., Park, R.-J., Holz, R., Kuehn, R.E., Eloranta, E., Knote, C., Jordan, C.E., Lefer, B.L., 2019. Meteorology influencing springtime air quality, pollution transport, and visibility in Korea. Elementa: Sci. Anthropocene 7 (1), 57.

Phillips, G.J., Thieser, J., Tang, M., Sobanski, N., Schuster, G., Fachinger, J., Drewnick, F., Borrmann, S., Bingemer, H., Lelieveld, J., Crowley, J.N., 2016. Estimating N_2O_5 uptake coefficients using ambient measurements of NO_3, N_2O_5, $ClNO_2$ and particle-phase nitrate. Atmos. Chem. Phys. 16 (20), 13231–13249.

Povey, I.M., South, A.M., de Roodenbeke, A.T.K., Hill, C., Freshwater, R.A., Jones, R.N., 1998. A broadband lidar for the measurement of tropospheric constituent profiles from the ground. J. Geophys. Res. 103, 3369–3380, 30.

Pusede, S.E., Duffey, K.C., Shusterman, A.A., Saleh, A., Laughner, J.L., Wooldridge, P.J., Zhang, Q., Parworth, C.L., Kim, H., Capps, S.L., Valin, L.C., Cappa, C.D., Fried, A., Walega, J., Nowak, J.B., Weinheimer, A.J., Hoff, R.M., Berkoff, T.A., Beyersdorf, A. J., Olson, J., Crawford, J.H., Cohen, R.C., 2016. On the effectiveness of nitrogen oxide reductions as a control over ammonium nitrate aerosol. Atmos. Chem. Phys. 16 (4), 2575–2596.

Ravishankara, A.R., 1997. Heterogeneous and multiphase chemistry in the troposphere. Science 276 (5315), 1058–1065.

Ren, X., Brune, W.H., Mao, J., Mitchell, M.J., Lesher, R.L., Simpas, J.B., Metcalf, A.R., Schwab, J.J., Cai, C., Li, Y., Demerjian, K.L., Felton, H.D., Boynton, G., Adams, A., Perry, J., He, Y., Zhou, X., Hou, J., 2006. Behavior of OH and HO_2 in the winter atmosphere in New York City. Atmos. Environ. 40, 252–263.

Riemer, N., Vogel, H., Vogel, B., Schell, B., Ackermann, I., Kessler, C., Hass, H., 2003. Impact of the heterogeneous hydrolysis of N_2O_5 on chemistry and nitrate aerosol formation in the lower troposphere under photosmog conditions. J. Geophys. Res. 108 (D4), 4144.

Seinfeld, J.H., Pandis, S.N., 1998. Atmospheric Chemistry and Physics. A Wiley-Interscience Publication.

Stull, R.B., 1988. An Introduction to Boundary Layer Meteorology. Springer, Dordrecht, Netherlands.

Wahner, A., Mentel, T.F., Sohn, M., 1998. Gas-phase reaction of N_2O_5 with water vapor: Importance of heterogeneous hydrolysis of N_2O_5 and surface desorption of HNO_3 in a large teflon chamber. Geophys. Res. Lett. 25 (12), 2169–2172.

Wang, X., Jacob, D.J., Eastham, S.D., Sulprizio, M.P., Zhu, L., Chen, Q., Alexander, B., Sherwen, T., Evans, M.J., Lee, B.H., Haskins, J.D., Lopez-Hilfiker, F.D., Thornton, J. A., Huey, G.L., Liao, H., 2019. The role of chlorine in global tropospheric chemistry. Atmos. Chem. Phys. 19, 3981–4003.

Wang, X., Jacob, D.J., Fu, X., Wang, T., Le Breton, M., Hallquist, M., Liu, Z., McDuffie, E. E., Liao, H., 2020. Effects of anthropogenic chlorine on $PM_{2.5}$ and ozone air quality in China. Environ. Sci. Technol. 54, 9908–9916.

Yun, C., Kim, J., Lee, J., Lee, J., Gil, J., Lee, M., Lee, G., 2024. Nocturnal downward transport of NO_3 radical from the residual layer to a surface site by the mountain breeze in Seoul, South Korea. Atmos. Environ. 321, 120345.

Zhang, B., Shen, H., Yun, X., Zhong, Q., Henderson, B.H., Wang, X., Shi, L., Gunthe, S.S., Huey, L.G., Tao, S., Russell, A.G., Liu, P., 2022. Global emissions of hydrogen chloride and particulate chloride from continental sources. Environ. Sci. Technol. 56 (7), 3894–3904.

Zhang, Q., Streets, D.G., Carmichael, G.R., He, K.B., Huo, H., Kannari, A., Klimont, Z., Park, I.S., Reddy, S., Fu, J.S., others, 2009. Asian emissions in 2006 for the NASA INTEX-B mission. Atmos. Chem. Phys. 9, 5131–5153.